



# Calibrating the Yield Strength of Archean Lithosphere Based on the Volume of Tonalite-Trondhjemite-Granodiorite Crust

Prasanna M. Gunawardana<sup>1\*</sup>, Gabriele Morra<sup>2</sup>, Priyadarshi Chowdhury<sup>1</sup> and Peter A. Cawood<sup>1</sup>

<sup>1</sup> School of Earth, Atmosphere and Environment, Monash University, Clayton, Victoria, Australia, <sup>2</sup> Department of Physics, School of Geosciences, University of Louisiana at Lafayette, Lafayette, LA, United States

## OPEN ACCESS

### Edited by:

Jeroen Van Hunen,  
Durham University, United Kingdom

### Reviewed by:

Kent Condie,  
New Mexico Institute of Mining and  
Technology, United States  
J. Elis Hoffmann,  
Freie Universität Berlin, Germany

### \*Correspondence:

Prasanna M. Gunawardana  
prasanna.gunawardana@  
monash.edu

### Specialty section:

This article was submitted to  
Solid Earth Geophysics,  
a section of the journal  
Frontiers in Earth Science

Received: 03 April 2020

Accepted: 24 August 2020

Published: 24 September 2020

### Citation:

Gunawardana PM, Morra G,  
Chowdhury P and Cawood PA (2020)  
Calibrating the Yield Strength of  
Archean Lithosphere Based on the  
Volume of Tonalite-Trondhjemite-  
Granodiorite Crust.  
Front. Earth Sci. 8:548724.  
doi: 10.3389/feart.2020.548724

Lithospheric yield stress is a key parameter in controlling tectonic processes. Using high resolution, 2D numerical modeling, we calculate the yield stress for a range of conditions appropriate to the early-to-mid Archean Earth, including hotter mantle potential temperatures and Moho temperatures. We then evaluate its effect on generating tonalite-trondhjemite-granodiorite (TTG) crust and benchmark the results against the preserved igneous rock record. Our results indicate that lithospheric yield stress values lower than the present-day values (i.e.,  $\leq 100$  MPa) can generate TTG volumes similar to those preserved in the rock record. The models further highlight the dominance of lithospheric dripping in producing the Archean TTGs. Large volumes of TTG melts form within the thin, tail portions of the drips as these regions are more efficiently heated by the enclosing hotter mantle. In contrast, only limited melting occurs within the thickened parts of lithosphere as they are significantly weak and cannot sustain crustal thickening for long time periods, resulting in its removal via dripping. This study, therefore, reaffirms the dominance of non-plate tectonic mechanisms in producing TTGs under the conditions that operated on the hotter Archean Earth.

**Keywords:** Archean, TTG, geodynamics, yield stress, dripping

## INTRODUCTION

Continental crust has played a key role in the evolution of the Earth system (e.g., Cawood et al., 2013). While its production is controlled by plate tectonics on the modern Earth (e.g., Rudnick and Gao, 2003), the tectonic processes that formed felsic crust and continents on the early Earth remain debated and range from plate tectonic to non-plate tectonic settings (e.g., Martin and Moyen, 2002; Bedard, 2003; Foley et al., 2003; Rapp et al., 2003; Harrison, 2009; Smithies et al., 2009; Chowdhury et al., 2017; Johnson et al., 2017; Moyen and Laurent, 2018; Rosas and Korenaga, 2018; Capitanio et al., 2019; Smithies et al., 2019; Chowdhury et al., 2020; O'Neill et al., 2020; Turner et al., 2020). This uncertainty partly stems from the significant gap in the preserved rock record and therefore, in our limited knowledge about the proportion and nature of the early continental and oceanic lithospheres (Cawood et al., 2013; Cawood et al., 2018; Lenardic, 2018; Stern, 2018). Numerical modeling of the early Earth processes and ground truthing its results with the limited rock record is, therefore, an important way to understand the early Earth processes (Rozel et al., 2017; Capitanio et al., 2019; Gerya, 2019; Chowdhury et al., 2020).

One approach to understand the Archean continental crust forming processes is by constraining the physical properties of the lithosphere(s) prevalent at that time. Previous research has shown that whether or not a terrestrial planet manifests some form of plate tectonics will depend on the lithospheric yield stress, i.e., the plastic strength of the crustal and the underlying lithospheric mantle rocks (Moresi and Solomatov, 1998; Trompert and Hansen, 1998; Tackley, 2000; O'Neill and Lenardic, 2007; van Heck and Tackley, 2008; Korenaga 2010a; Korenaga, 2010b; Van Heck and Tackley, 2011). Based on the magnitude of this parameter, a planet can exist in stagnant-lid, episodic-lid or mobile-lid tectonic mode (Moresi and Solomatov, 1998), since changing the yield stress value affects the mantle convection pattern via affecting the viscosity contrast between the lithosphere and convecting mantle. For example, present-day continental crust production mainly occurs at subduction and orogenic settings within a plate tectonic (mobile-lid) regime where average lithospheric yield stresses vary within >100–150 MPa (Kohlsted et al., 1995; Gurnis, 1988; Lowman and Jarvis, 1999; Tackley, 2000). However, this parameter remains poorly constrained for the Archean lithosphere.

Here, we perform high resolution 2D numerical modeling of the lithospheric dynamics under hotter mantle conditions appropriate for the early-to-mid Archean (>3 Ga) time-period, for a range of yield stress values varying between 50 and 250 MPa. We evaluate the models by calibrating the tempo of granitoid formation as obtained from them with the preserved geological record, and thereby, seek to constrain the yield stress values of Archean lithosphere and the consequent tectonic settings responsible for the formation of early felsic crust. Changes in the lithospheric processes due to different yield stress values are likely to affect the pressure-temperature ( $P$ - $T$ ) conditions of tectonic environments where metamorphism and partial melting processes operate. This implies that yield stress values are implicitly linked to the formation conditions and volumes of Archean felsic crust, which can be independently constrained from other approaches, thus, can be used to trace it back for the ancient lithosphere.

## METHODOLOGY

### Numerical Methods

We model 2D-mantle convection at high mantle potential temperatures ( $T_p$ ; ~1,475–1,600°C) inferred for the Archean (Herzberg et al., 2007; Herzberg et al., 2010; Korenaga, 2013; Ganne and Feng, 2017; Aulbach and Arndt, 2019) using the numerical code Underworld 2 (Moresi et al., 2007). This code is based on the finite element method and is coupled with the particle-in-cell approach (Evans and Harlow, 1957). It involves a Eulerian grid with the moving Lagrangian particles embedded in a finite element (Moresi et al., 2007). Each particle represents a specific solid or molten rock-type (termed as *rock-particle* hereafter) and carries the information about its physical properties like,  $P$ ,  $T$ , density, etc., which can be tracked over the entire model duration. The mass, momentum, and energy conservation equations are

solved under incompressible conditions to find the pressure, velocity, and thermal evolution of the mantle convection model. Physical properties such as density and viscosity associated with the Earth's interior are mapped to these equations through particle indexing. The mass, momentum, and energy conservation equations are:

$$\vec{\nabla} \cdot \vec{u} = 0 \quad (1)$$

$$-\vec{\nabla} \cdot P + \vec{\nabla} \cdot [\eta(\partial_i u_j + \partial_j u_i)] = -\rho \vec{g} \quad (2)$$

$$\partial_t T + \vec{u} \cdot \vec{\nabla} T = \nabla^2 T + H \quad (3)$$

where  $u$ ,  $P$ ,  $\eta$ ,  $T$ ,  $H$ ,  $\rho$ ,  $g$ , and  $t$  represent velocity, pressure, viscosity, temperature, internal heat, density, gravitational acceleration, and time, respectively, (see **Table 1** for the parameter values).

The temperature dependent diffusion creep rheology is applied using the Arrhenius equation (Rozel et al., 2017):

$$\eta_T = \eta_o \exp \left[ \frac{E + d \cdot V}{T + 1} - \frac{E}{2} \right] \quad (4)$$

where  $\eta_o$  is the reference viscosity at  $T = 1$ . Here, the parameters  $E$ ,  $V$ , and  $d$  represent the non-dimensional activation energy, activation volume, and depth coordinate of the model, respectively. Following some recent studies (e.g., Sizova et al., 2015; Rozel et al., 2017), the activation energy is applied in such a way that temperature dependent rheology creates a stagnant lid mode of convection in the model (Moresi and Solomatov, 1998). A lithospheric weakening mechanism is implemented using the yield stress ( $\sigma_Y$ ) parameter by assuming the ductile (plastic strength) behavior of the lithospheric rocks (Moresi and Solomatov, 1998; Sizova et al., 2015; Rozel et al., 2017). This is the only weakening mechanism that we imposed in the model. The yield stress equation is:

$$\sigma_Y = \sigma_Y^o + d\sigma_Y' \quad (5)$$

where  $\sigma_Y^o$  is Earth's surface yield stress and  $\sigma_Y'$  is the depth dependent yield stress gradient. When the convective stresses exceed the yield stress, we choose the yield stress value to calculate the viscosity. The yielding viscosity is  $\eta_Y = \sigma_Y/2\dot{\epsilon}$ , where  $\dot{\epsilon}$  is the second invariant of the strain rate tensor. The effective viscosity is then calculated by  $\eta_e = [\eta_T^{-1} + \eta_Y^{-1}]^{-1}$ . We have systematically varied the surface yield stress among the values of 50, 100, 150, 200, and 250 MPa, covering a range of weaker to stronger lithospheric strength profiles. These values are proximal to the yield stress compatible with plate tectonics (Moresi and Solomatov, 1998; Tackley, 2000a; Van Heck and Tackley, 2011).

The dimensional values of the above non-dimensional parameters are retrieved using the relationships:

$$t = \frac{d^2}{k} t', \quad \sigma = \frac{\eta_o k}{d^2} \sigma', \quad x_i = dx'_i, \quad u_i = \frac{k}{d} u'_i, \\ \eta = \eta_o \eta', \quad \text{and} \quad T = \Delta T T'$$

following scaling methods of Moresi and Solomatov (1998), Korenaga (2010b), and Van Heck and Tackley (2011). The primes represent the non-dimensional form of the variable

**TABLE 1** | Physical properties used in numerical modeling.

Symbol	Definition	Non-dimensional value	Dimensional value
$\alpha$	Thermal expansivity	$10^7$	$3 \times 10^{-5}$ 1/K
$g$	Gravitational acceleration	1	9.81 m/s <sup>2</sup>
$d$	Mantle thickness	1	660 km
$T_o$	Surface temperature	0	0°C
$\Delta T$	Temperature drop across the model	Vary based on $T_p$ (1 for present Earth)	1,680°C for present Earth
$\rho_o(\text{peri})$	Reference density for peridotite	1	3,300 kg/m <sup>3</sup>
$\rho_o(\text{basalt})$	Reference density for basalt	—	3,000 kg/m <sup>3</sup>
$\rho_o(\text{TTG})$	Reference density for TTG	—	2,700 kg/m <sup>3</sup>
$\kappa$	Thermal diffusivity	1	$10^{-6}$ m <sup>2</sup> /s
$\eta_o$	Reference viscosity	1	$10^{21}$ Pa s
$E$	Activation energy	—	270 kJ/mol
$R$	Universal gas constant	—	8,314 J/mol/K
$\sigma'_Y$	Yield stress gradient	$10^7$	~35 MPa/km

and will be dropped here onwards, as we will only be dealing with non-dimensional symbols.

### Partial Melting

To model felsic and mafic crust production, we implemented partial melting of the mantle peridotite and basaltic crust, including melt extraction, residue formation and eclogitization.

For any rock-particle, melting initiates whenever its temperature exceeds its solidus. The adiabatic component of the temperature is added to the temperature solution ( $T$ ) of Eq. 3 for the melt calculation. The  $P$ - $T$  dependent peridotite melting model of Sizova et al. (2015) is used for the mantle melting and melt extraction processes to account for the realistic scenario of mantle melting over a range of temperature between its wet and dry

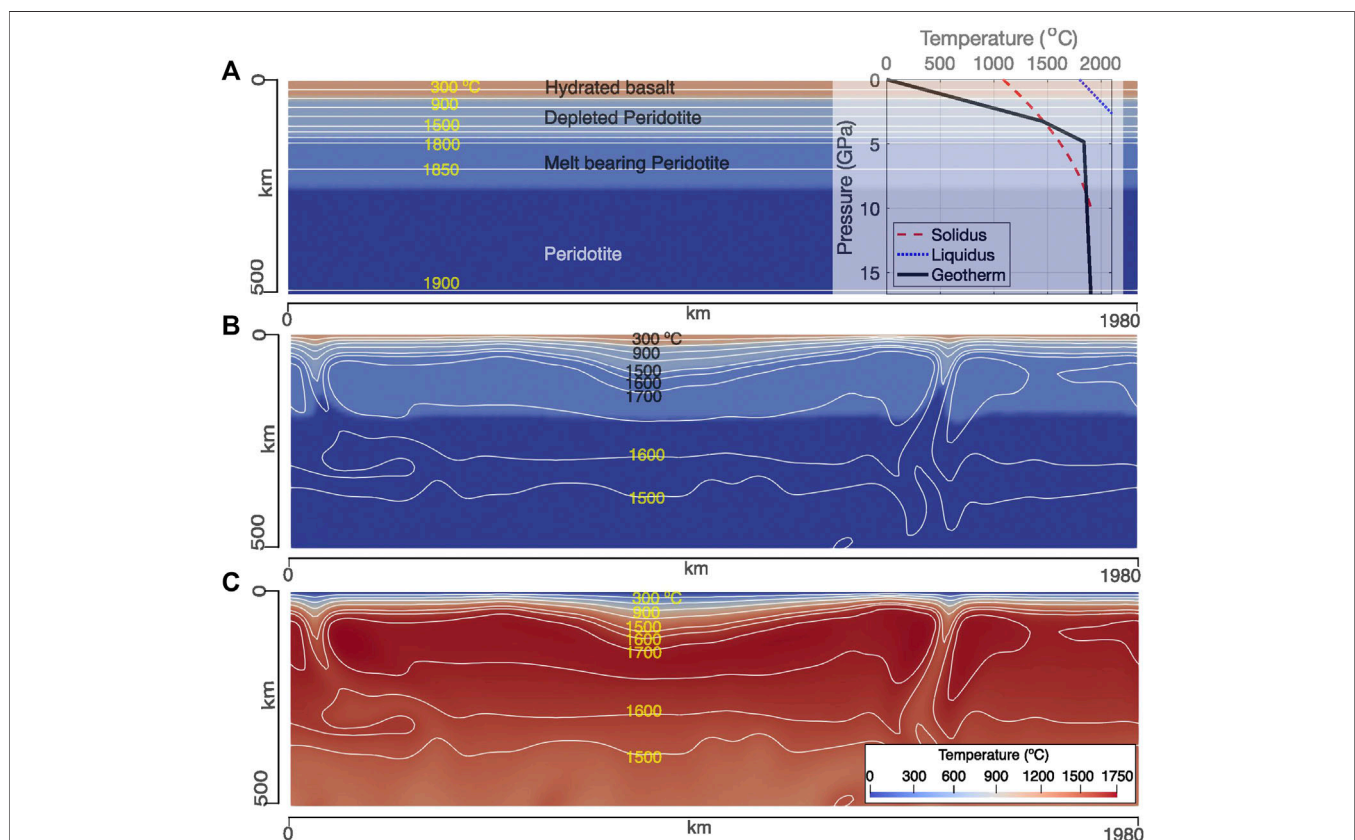


**FIGURE 1** | (A) The initial compositional setup used to reach a state of stable mantle convection. The geotherm corresponds to a mantle  $T_p$  of 1,600°C and mantle adiabat of 0.5°C/km. The thickness of basaltic crust is defined by a Moho- $T$  of 600°C. (B,C) The compositional and thermal profile derived after a stable mantle convection pattern is established. The lithological particles in (B) has been redefined using the thermal profile shown in (C). This stage is considered as the start of model evolution for calculating the volume of tonalite-trondhjemite-granodiorite crust.

solidus depending on the extent of hydration. For the basaltic crust, the volumetric degree of melting, i.e., melt-fraction ( $M_o$ ) is considered as a linear function of  $P$ - $T$  and is calculated using the equation (Gerya, 2010; Sizova et al., 2015; Chowdhury et al., 2017; Chowdhury et al., 2020):

$$M_o = \begin{cases} 0, & T_1 < T_{\text{solidus}} \\ \frac{T_1 - T_{\text{solidus}}}{T_{\text{liquidus}} - T_{\text{solidus}}}, & T_{\text{solidus}} < T_1 < T_{\text{liquidus}} \\ 1, & T_1 > T_{\text{liquidus}} \end{cases} \quad (6)$$

where  $T_{\text{solidus}}$  and  $T_{\text{liquidus}}$  represent solidus and liquidus temperatures (Figure 1; also see Appendix) and are taken from the previous studies (e.g., Sizova et al., 2015; Rozel et al., 2017; Chowdhury et al., 2020). The melting of felsic crust has not been considered here.

To extract melt from partially-molten lithologies, we define four threshold parameters ( $M1$ ,  $M2$ ,  $M3$ , and  $M4$ ) following the algorithm of Sizova et al. (2015) for each rock-particle.  $M1$  represents the non-extractable melt volume that always remains in a partially molten rock-particle, while  $M2$  represents the minimum melt volume required for the melt-extraction to take place. The extracted melt volume is assumed to instantaneously leave the melting region and move to the surface (Schmeling, 2006).  $M3$  is the maximum amount of melt that can be sustained in a crystallizing melt particle without melt fractionation.  $M4$  is the maximum amount of cumulative melt that can be extracted from a rock-particle. Once a rock-particle melts beyond  $M4$ , it is considered infertile for further melting. All the threshold parameters are assigned distinct values according to the rock-type (mantle peridotite or basalt; see Appendix A1). The melt volume borne by a rock-particle at any instant of time ( $M$ ) during the model evolution is given by:  $M = M_o - \sum_n M_{\text{ext}}$  where,  $M_o$  is given Eq. 6,  $M_{\text{ext}}$  is the amount of melt extracted in a single time-step and  $n$  is the number of times melt has been extracted from that rock-particle ( $\sum_n M_{\text{ext}}$  gives the total melt-fraction extracted from that rock-particle). Whenever  $M$  exceeds  $M2$  for a rock-particle, the extracted melt fraction ( $M_{\text{ext}}$ ) is calculated as  $M - M1$ . This value is then added to the extracted cumulative volume of extracted melt for that rock-particle, which is then compared to  $M4$  to check whether that rock-particle has reached its final limit for melt-extraction or not. The prefix *melt-bearing* is attached to the lithological name of a rock-particle (e.g., melt-bearing peridotite) whenever it carries some melt ( $M > 0$ ). Once the cumulative melt-volume reaches  $M4$ , the melt-bearing rock-particle is converted to an equivalent depleted lithology like, from melt-bearing peridotite to depleted peridotite.

## Density Calculations

The temperature dependent density ( $\rho$ ) for different rock types is calculated using:  $\rho_o [1 - \alpha \Delta T]$  where the  $\rho_o$  is the reference density at 1 MPa and 298 K,  $\alpha$  is the thermal expansivity, and  $\Delta T$  is the temperature drop across the model (Table 1). Partial melting and melt extraction also affect the density of the

resultant rock types. The effective density of a melt-bearing rock type is calculated using (Gerya, 2010):

$$\rho_{\text{eff}} = \rho_{\text{solid}} (1 - M) + \rho_{\text{melt}} M \quad (7)$$

While  $\rho_{\text{melt}}$  represents the temperature dependent density of the melt volume ( $M$ ),  $\rho_{\text{solid}}$  is the density of the solid part of the melt-bearing rock-types - called residue - that includes the effect of temperature, melt-extraction and eclogitization. It is calculated using:

$$\rho_{\text{solid}} = \rho_o [1 - \alpha \Delta T] (1 + \text{coef}_{\text{res}} + \text{coef}_{\text{phase}}) \quad (8)$$

where  $\text{coef}_{\text{res}}$  and  $\text{coef}_{\text{phase}}$  represent the coefficients of density changes due to melting and eclogitization, respectively.

The density of solid peridotite decreases due to melt depletion (e.g., Poudjom Djomani et al., 2001), which we have implemented using the relation:  $\text{coef}_{\text{res}} = -0.04 \sum_n M_{\text{ext}}$  (Sizova et al., 2015). This corresponds to a decrease of ~1% in the density of solid residual peridotite for every 25% of extracted melt volume. For depleted peridotite (i.e.,  $M = M4$ ),  $\rho_{\text{solid}}$  is calculated at a fixed  $\sum_n M_{\text{ext}}$  of 40%. No phase transitions are considered for the mantle peridotite ( $\text{coef}_{\text{phase}} = 0$ ). During the melting of a metabasalt at amphibolite facies, the residue becomes rich in garnet, which makes it denser than the unmetamorphosed basalt (Rapp et al., 2003; Zhang et al., 2013). This effect is modeled using the following relation:  $\text{coef}_{\text{res}} = 0.4 \sum_n M_{\text{ext}}$  (Sizova et al., 2015). The effect of phase transitions, i.e., eclogitization on the basaltic density is implemented via the term  $\text{coef}_{\text{ec}}$ . Following the experimental results (Ito and Kennedy, 1971), the values of this coefficient are varied from 0 to 16% within the  $P$ - $T$  dependent garnet-in line [ $P$  (in kbar) = 0.014  $T$  (in °C) - 5.4] and plagioclase-out line [ $P$  (in kbar) = 0.024  $T$  (in °C) + 4] (Sizova et al., 2015), which approximates the conversion of basalt to eclogite through garnet-granulite. It must be noted that eclogitization is not necessarily dependent of melting and therefore, its effect on density is calculated for all the basaltic rock-particles (both solid and melt-bearing).

## Initial Setup and Boundary Conditions

Our 2D model domain is created with a  $64 \times 192$  resolution Eulerian mesh and with 20 Lagrangian particles per cell. The model dimension is 660 km  $\times$  1,980 km (Figure 1A). A lithosphere with thick, hydrous basaltic crust is used in the models (Figure 1A) in accordance to the recent geological findings (e.g., Herzberg et al., 2010; Herzberg and Rudnick, 2012; Kamber, 2015; Johnson et al., 2017). The crustal thickness is set by the Moho temperature (Moho- $T$ ). Whenever a rock-particle exists within the upper 60 km of the model domain and its temperature is less than Moho- $T$ , it is defined as basaltic crust. We varied the crustal thickness using three different values of Moho- $T$  (500, 600, and 700°C). The relevant average basaltic crustal thickness for the model with mantle  $T_p$  1,600°C and yield stress of 50 MPa case is presented in Appendix Figure A1. These different Moho- $T$  values also simulate the effect of relatively colder and hotter crustal geotherms. Following the studies of Rey et al. (2014) and Sizova et al. (2015), the lithospheric thickness is thermally

defined by 0°C at the surface and a temperature at a fixed depth of 100 km depending on the mantle  $T_p$  values. We further increased the mantle  $T_p$  value by 125, 200, and 250°C above its present-day value of 1,350°C in successive steps, which are consistent with the thermal conditions of Archean mantle (Herzberg et al., 2010; Korenaga, 2013). The ambient mantle temperature linearly increases following an adiabatic geotherm of ~0.5°C/km below 150 km depth. Above 150 km, the mantle adiabat is linearly linked to the lithospheric geotherm over the depth interval of 100–150 km (Figure 1A). The top boundary is kept constant at 0°C while the bottom boundary is kept at constant temperature guided by the mantle  $T_p$  and the mantle adiabatic geothermal gradient (see Table 1). Free slip boundary conditions are imposed at the top and bottom of the model, while side walls are given periodic boundary condition. We have run all the models for a finite time at the beginning to reach a steady-state mantle convection (Figure 1C). Once this is achieved, the lithological layers are redefined according to the established steady-state thermal profile (Figure 1B). The stage is considered as the start of the model evolution.

## Constraints From the Continental Rock Record

To evaluate our models, we predict the 1) relative abundances of various felsic igneous rocks and 2) the volume of continental crust that would have been formed during the early Archean (>3 Ga), and compare them against the volumes inferred from the rock record.

### Comparison with the rock record of Tonalite-Trondhjemite-Granodiorites

To evaluate our models, we need information about the relative abundances of the different types of Tonalite-Trondhjemite-Granodiorite (TTG) - the dominant felsic lithologies that constitute Archean crust (reviewed in Moyen, 2011; Moyen and Laurent, 2018). Extant experimental and petrological studies show that the Archean TTGs mainly formed through the partial melting of hydrated metabasalts (Foley et al., 2003; Rapp et al., 2003; Moyen and Stevens, 2006; Qian and Hermann, 2013; Palin et al., 2016; Johnson et al., 2017). Our implemented algorithm of basalt melting is, thus, appropriate to model TTG formation. The trace element composition of TTGs further suggest that their formation occurred at three different pressure ranges: (Moyen, 2011): 1) at lower pressures (<1 GPa) where garnet-absent amphibolite residues are stable, called low-pressure (LP-) TTGs; 2) at intermediate pressures (~1–2 GPa) where both garnet and plagioclase are present in the residue, called medium-pressure (MP-) TTGs; and 3) at high pressures (>2 GPa) where garnet and rutile are stable in the residue but not plagioclase, called high-pressure (HP-) TTGs. The bracketing pressure ranges, however, may vary depending on the source rock composition; for example, MP-TTGs can form at  $P < 1$  GPa (~0.7–0.8 GPa) from low-MgO enriched metabasalts (Johnson et al., 2017).

In this study, we focus on the formation of LP- and MP-TTGs as they dominate the >3 Ga rock record (cf. Moyen and

Laurent, 2018), which is the time period of interest. We modeled partial melting of hydrous basaltic crust within a pressure range of 0.7–2.5 GPa, corresponding to a maximum depth of ~75 km (Figure 2). Notwithstanding the ambiguities of nomenclature, this pressure range overlaps with the overall physical conditions of LP- and MP-TTGs formation during the Archean (Figure 2) (Palin et al., 2016; Johnson et al., 2017; Moyen and Laurent, 2018). Regarding the relative abundances, MP-TTGs constitute nearly 60% of the total TTG volume whereas LP- and HP-TTGs contribute equally toward the remaining 40% (Moyen, 2011; Moyen and Laurent, 2018). Since we focus on the LP- and MP-TTGs, we renormalize their proportions and obtain a ratio of 1:3 (~25%:75%) between their abundances. Whenever a basaltic rock-particle melts, the resultant melt is classified as LP-/MP-/HP-TTG depending on in whose domain the melting took place (Figure 2). Melt is extracted once the melt-fraction reaches the threshold limit for extraction ( $M_2$ ) as mentioned above. The extracted melt volumes for each of the TTG-types are computed at each time step and added to the volumes of the previous time-steps. It must be noted that we did not consider water and basalt as separate entities and instead, assumed the basaltic crust to be sufficiently hydrated to produce the different TTG-types (e.g., Sizova et al., 2015; Chowdhury et al., 2020).

### Comparison with the volume of ~3 Ga old continental crust

Comparing the total continental crustal volume between models and nature is not straightforward, particularly because of the large variations among different growth models and the difficulties in extrapolating the numerical model results at planetary scales. Estimates for the volume of continental crust at ~3 Ga vary from ca. 10 to 120% of its present-day volume between the different growth models (Figure 3) (cf. Cawood and Hawkesworth, 2019). This is because these models are based on different assumptions and datasets. While some growth models are based on the present-day distribution of the continental crust (e.g., Condie and Aster, 2010), some others are schematic (e.g., Armstrong, 1981). A third group of growth models also exist that are based on datasets such as the proportions of juvenile vs. reworked crust inferred from the zircon data, the evolution of atmospheric argon, and the trace element and isotopic composition of mafic-ultramafic rocks (Campbell, 2003; Belousova et al., 2010; Dhuime et al., 2012; Pujol et al., 2013; Roberts and Spencer, 2015; McCoy-West et al., 2019). Here, we consider the volume estimates of this group of growth models since: 1) they do not rely on the present-day crustal distribution; thus, accounting for the current paucity of the early rock record and 2) they all independently show that at least 65–70% of the present-day continental volume existed by ~3 Ga. It must be noted that besides granitoids, the Archean continental crust is also comprised of greenstone belt successions made up of mafic-ultramafic volcanic and volcanoclastic rock units (Moyen and Laurent, 2018; Smithies et al., 2018). The estimates of continental growth models are however, meant for the felsic component mainly (Dhuime et al., 2012; Pujol et al., 2013; cf.; Cawood et al., 2013).

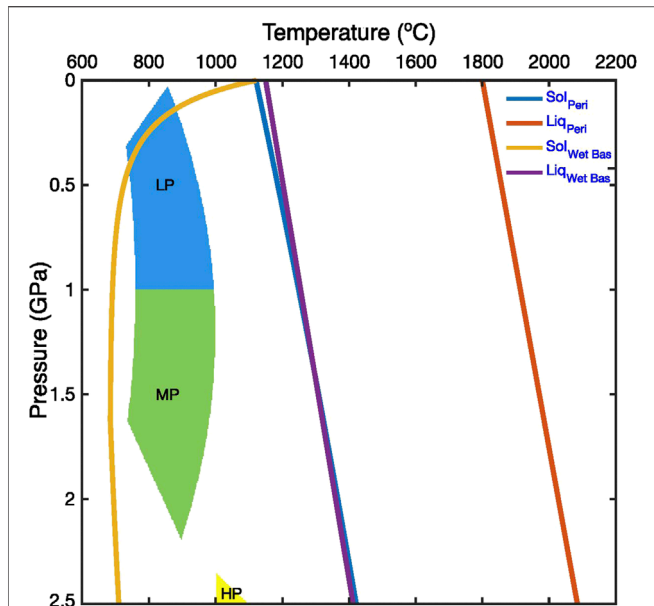


**FIGURE 2** | Pressure and temperature conditions of Low-Pressure (LP), Medium-Pressure (MP) and High-Pressure (HP) tonalite-trondhjemite-granodiorite formation (Reproduced from Moyen (2011) and Jain et al. (2019) under the Creative Commons CCBY license). The solidii and liquidii for mantle peridotite and hydrous basaltic crust (Sizova et al., 2015) are also shown. See **Appendix** for details.

To measure crustal growth within our models, we introduce a parameter called the *Differentiation Index* (DI). Defined as the volume ratio of the continental crust to the upper mantle, this parameter quantifies how much continental crust has been extracted from the mantle and did not mix back (at least

chemically); thus, accounting for the crustal recycling implicitly. Our approach follows the geochemical hypothesis that effectively continental crust has been extracted from the mantle (e.g., Rudnick and Gao, 2003). The DI value is estimated to be  $\sim 2.4\%$  for the modern Earth. It is calculated using the continental volume of  $\sim 7.2 \times 10^9$  km (cf. Cawood et al., 2013) and an upper mantle volume of  $\sim 3.03 \times 10^{11}$  km (based on a spherical Earth of radius 6,371 km and an upper-lower mantle boundary at the depth of 660 km). The DI value at  $\sim 3$  Ga is  $\sim 1.7\%$ , which is calculated assuming the continental crustal volume to be  $\sim 70\%$  of the present-day volume and the same upper mantle volume. During the model evolution, we compute the total volume of TTG crust formed at each time-step (as mentioned above). We then use this accumulated TTG volume to compute DI at each time-step and trace over what duration its inferred value of  $\sim 1.7\%$  is achieved.

## MODEL RESULTS

**Figure 4** illustrates the evolutionary stages of our reference numerical model, which has a surface yield stress of 50 MPa, a mantle  $T_p$  of  $1,600^\circ\text{C}$  ( $250^\circ\text{C}$  higher than present-day), and a Moho- $T$  of  $600^\circ\text{C}$ . The model evolution shows that two tectonic processes featuring local compression, called crustal thickening and dripping, occur under the influence of the convective flow of mantle. Thickening of the basaltic crust (**Figure 4A**) leads to phase transitions (i.e., eclogitization) within its deeper levels, which in turn increases the crustal density at those depths. Owing to a hotter geotherm set up by the hotter mantle and low yield stress, the crust could not support its gravitationally unstable eclogitized base and leads to the development of a Rayleigh-Taylor type instability within this region (**Figure 4B**).

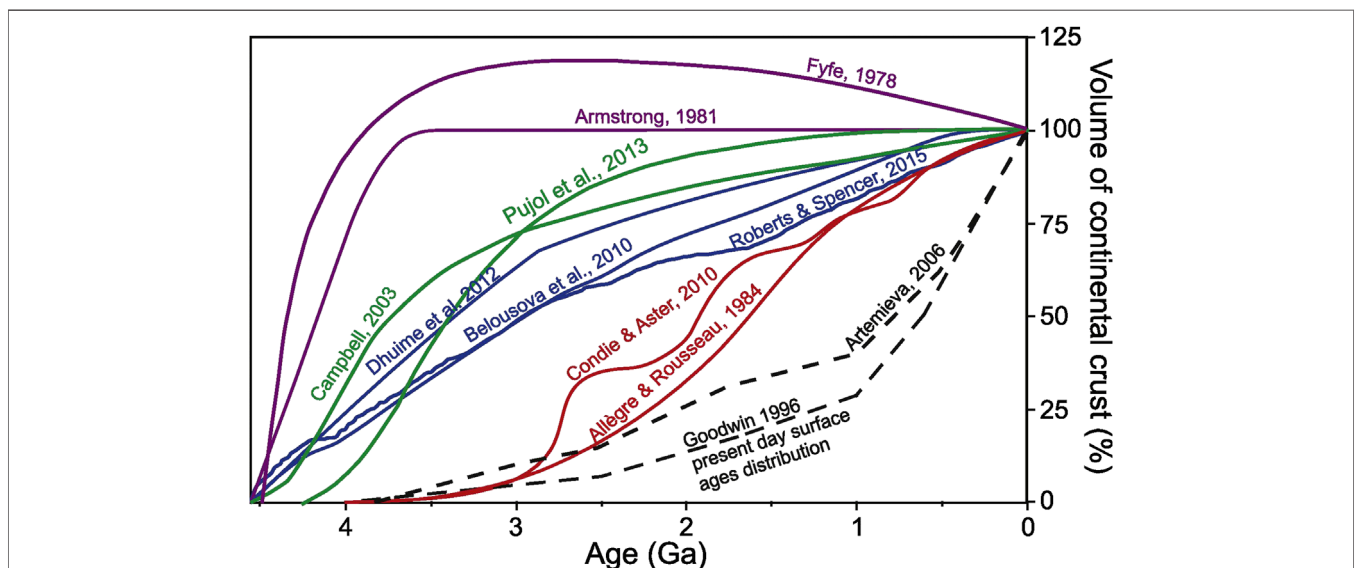


**FIGURE 3** | The growth models of the continental crust relative to its present-day volume (Reproduced from Cawood and Hawkesworth (2019) under the Creative Commons CCBY license). Note that the curves of Belousova et al. (2010), Dhuime et al. (2012), Roberts and Spencer (2015), Campbell (2003), Pujol et al. (2013), all of which used different proxies, predict similar volumes of continental crust at  $\sim 3$  Ga.

As this instability grows with time, a portion of the eclogitized crust drips back into the mantle (**Figures 4C,D**). Such a process has been suggested to occur during the early Archean by previous studies (Johnson et al., 2014; Sizova et al., 2015; Rozel et al., 2017). Our model however, shows that: 1) individual drips may grow in length, reaching up to few hundreds of km (**Figures 4A–D**) and 2) individual dripping phases, i.e., from the appearance of the Rayleigh-Taylor instability to the detachment stage, may last for ~10 Myr. The cycle of crustal thickening evolving into dripping continue to occur over a periodicity of ~20–30 Myr.

Regarding the formation felsic crust, the model shows that drips are more efficient in producing TTGs as compared to the basal part of a thickened crustal segment (cf. **Figures 4A–D**). The narrow tail region of a basaltic drip easily reaches supra-solidus temperatures due to the conductive heating from the surrounding hot mantle, resulting in its melting and the formation of TTGs. It must be noted that in our models we

have shown the residues (pink colored lithology) formed after the production of TTGs. Therefore, although residues get transported at great mantle depths with the drips (**Figures 4C,D**), they have necessarily formed at depths <75 km since we did not allow melting of the basaltic crust beyond this depth limit. **Figure 5** shows how the volumes of modeled LP-TTG and MP-TTG melts as well as their combined volume increase with time during the model evolution. The relative proportions of LP- to MP- TTG melts remain fairly constant (varying from ~22%:78% to ~30%:70%) around the ~1:3 ratio throughout the model evolution (**Figure 5B**), which agrees well with the rock record (Moyen, 2011; Moyen and Laurent, 2018). In terms of the absolute volume, prominent spikes implying significant growth in the TTG volume, can be seen at ~17.5, 56.8, and 100 Myr in the melt volume vs. time plot (**Figure 5A**). Notably, all these time-instants correspond to the active phases of dripping (**Figure 5C**). In contrast, melt volumes do not show any major increase when crustal thickening dominates the model

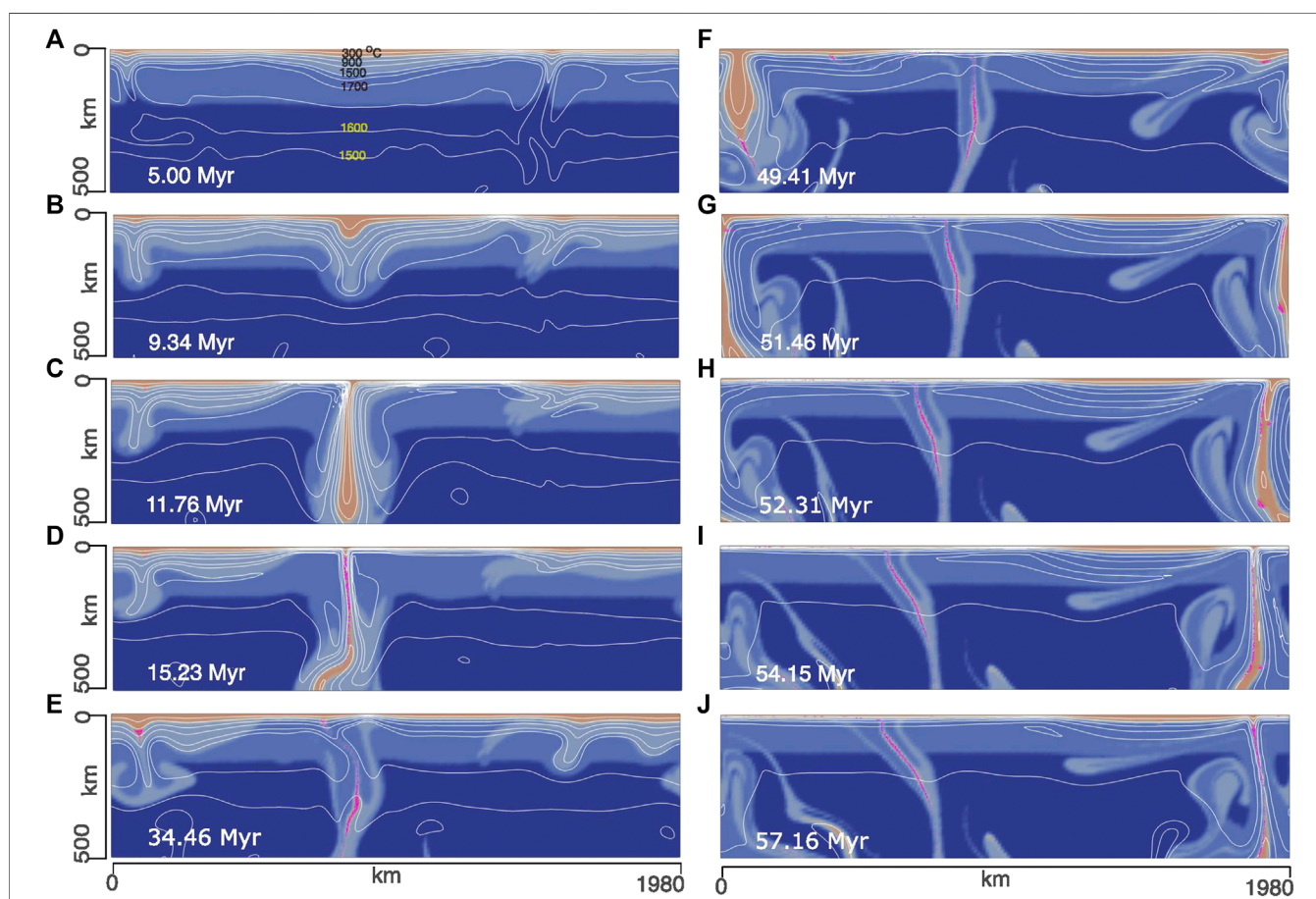


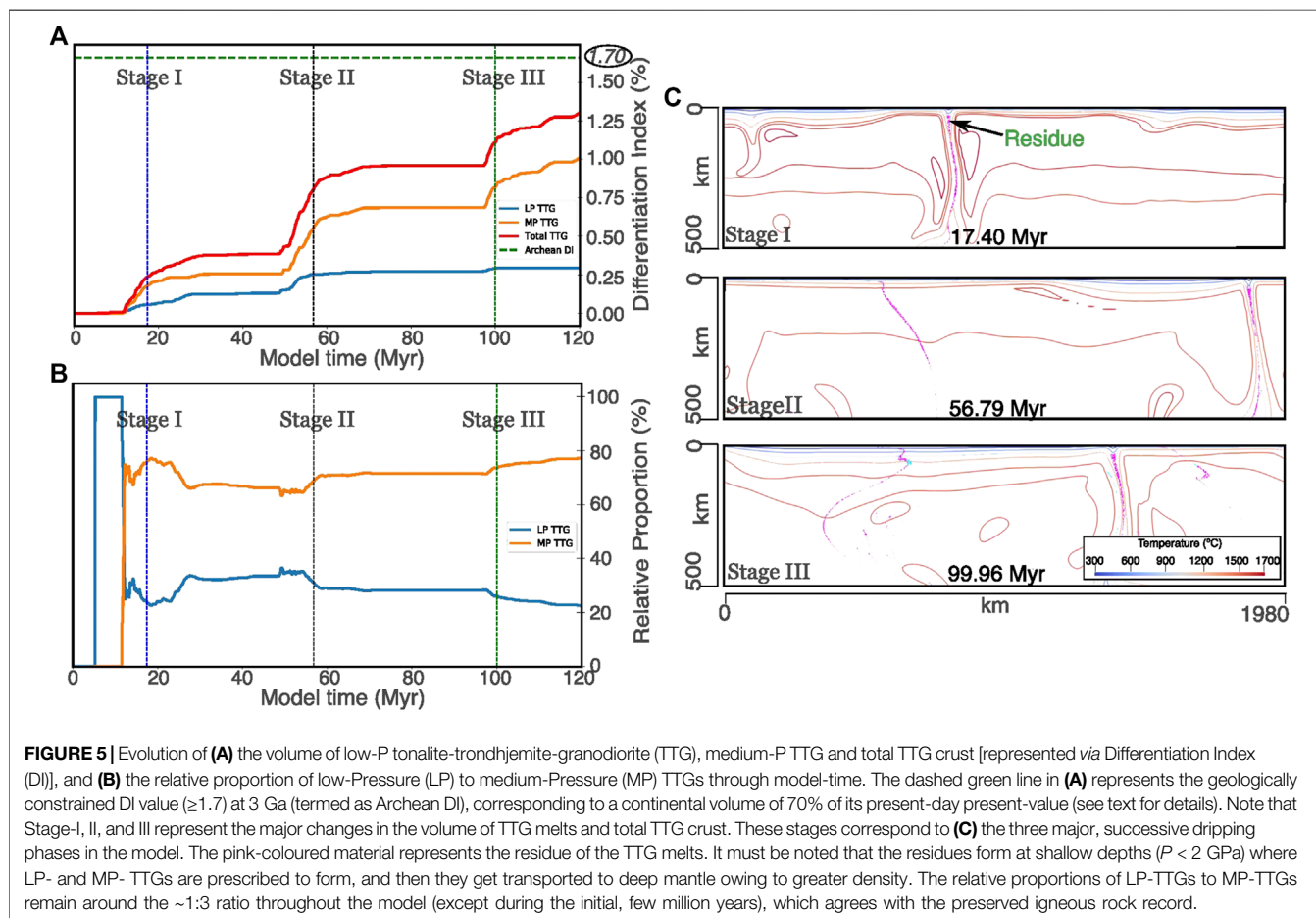
**FIGURE 4** | Evolution of the reference model with a surface yield stress of 50 MPa, mantle  $T_0$  of 1,600°C and Moho-T of 600°C. Mantle convection drives thickening of the basaltic crust (**A**), which eventually transform into a Rayleigh-Taylor type instability (**B**) and drips into the mantle (**C–E**). This cycle of crustal thickening followed by dripping continues. The residue forms during the production of tonalite-trondhjemite-granodiorite melt is shown in pink color. Within a period of ~60 Myr, the model shows two major dripping phases: the first phase (**B–E**) between ~9 and 34 Myr and the second phase (**F–J**) between ~49 and 57 Myr. Note that this second phase is transferred across the (periodic) boundary from left to right in the model (**G–H**) around the ~51–52 Myr time-period. The TTG formation mostly occurs during the dripping phase as compared to the thickening phase.

evolution (Figure 5A), implying only limited mafic crustal melting in this setting.

To test the effects of higher yield stress and Moho-T, we have simulated a model with a surface yield stress of 200 MPa and a Moho-T of 700°C under the mantle  $T_p$  of 1,600°C. This model also feature dripping (Figures 6A–C) and crustal thickening phases (Figures 6C–F) similar to the reference model. But, in this model, crustal thickening phases exhibit melting of the basaltic crust and TTG production in noticeable volumes (Figures 6E,F). A higher Moho-T along with a higher yield stress value leading to sustaining of thickened crustal domains over ~20–30 Myr, facilitates melting at the base of the thickened basaltic crust. This substantiates our contention that Moho-T and yield stress values together influence the production of TTGs within thickened crustal domains. However, even within this setup, the overall volume of the TTGs is controlled by the melt produced during the dripping phase (Figures 6A–G). However, the relative proportion of modeled LP- to MP-TTG melt do not corroborate to the desired value of ~1:3, rather they show sub-equal abundances (Figure 6H). Models with other values of yield stress, Moho-T and mantle  $T_p$  do not show any major deviation in their evolution from that of the reference model.

Furthermore, the model results show that TTG production and the resulting DI values increase with the lowering of

lithospheric yield strength for any given mantle and Moho temperature conditions (Figure 7). When the mantle  $T_p$  range is within 1,500–1,600°C, only the models having a lithospheric yield stress of ~50 to <100 MPa produces enough TTG volume such that their DI values approach or surpass the geological constrained DI value (~1.7%) of the Earth approximately at 3 Ga within few hundreds of Myr (Figures 7A,B). However, at low yield stresses, the DI reaches ~1.5–1.7% within  $\leq 100$  Myr when the Moho-T is 700°C irrespective of the mantle  $T_p$  (Figures 7A–C), implying an extremely rapid growth of felsic crust. In contrast, the DI values reach ~0.5–1.2 in 100 Myr when the Moho-T is ~600°C (Figures 7A–C); thereby, suggesting that the felsic crust grows steadily under these conditions and the DI values likely reach the ~1.7% value in a few hundreds of Myr. A colder Moho (~500°C) or mantle (<1,500°C  $T_p$ ) seems to limit the TTG production such that the DI values remain <0.5 in 100 Myr (Figures 7A–C); thus, favoring a slow crustal growth. However, the estimated DI values likely reach the ~1.7% in less than 1.5 Gyr for colder Moho (~500°C) and/moderate  $T_p$  (~1,540°C) and/higher yield stress (250 MPa) suggesting that slow crustal growth rates require excessively high lithospheric yield stress values. Even when the relative proportion of LP- and MP-TTGs are considered (Figures 7D–F), models with a combination of hotter mantle (>1,550°C  $T_p$ ), moderately high



Moho-T ( $\sim 500\text{--}600^\circ\text{C}$ ) and low lithospheric yield stresses ( $<150\text{ MPa}$ ) provide the best agreement to the natural rock-record. A significantly hotter Moho ( $\geq 700^\circ\text{C}$ ; **Figures 7D–F**) or colder mantle ( $<1,500^\circ\text{C } T_p$ ; **Figure 7F**) would strongly favor or disfavor the production of LP-TTGs, respectively, (even for weak lithosphere), which in turn deviates the ratio of LP- to MP-TTGs from their geologically constrained value ( $\sim 1:3$ ).

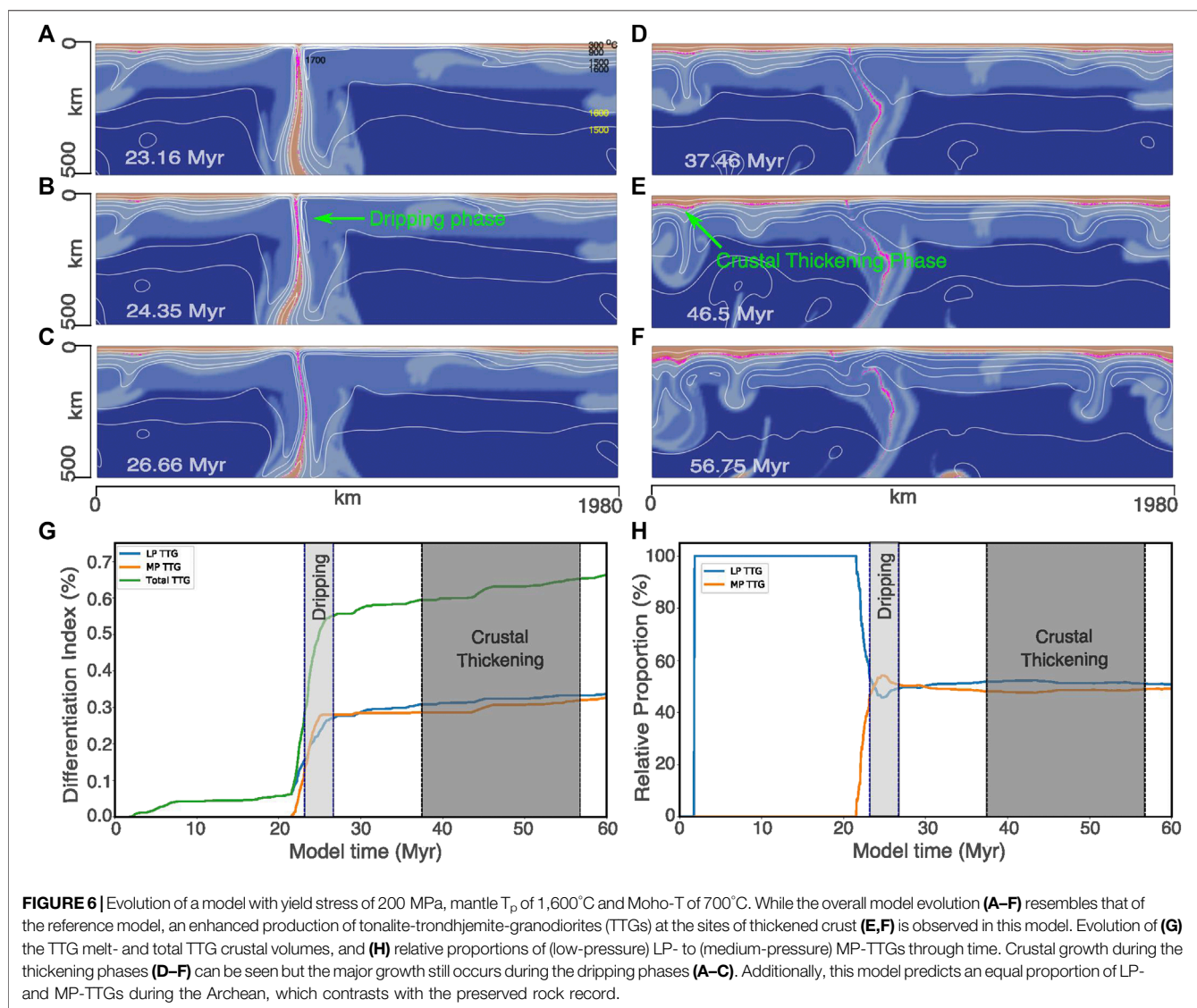
## DISCUSSION

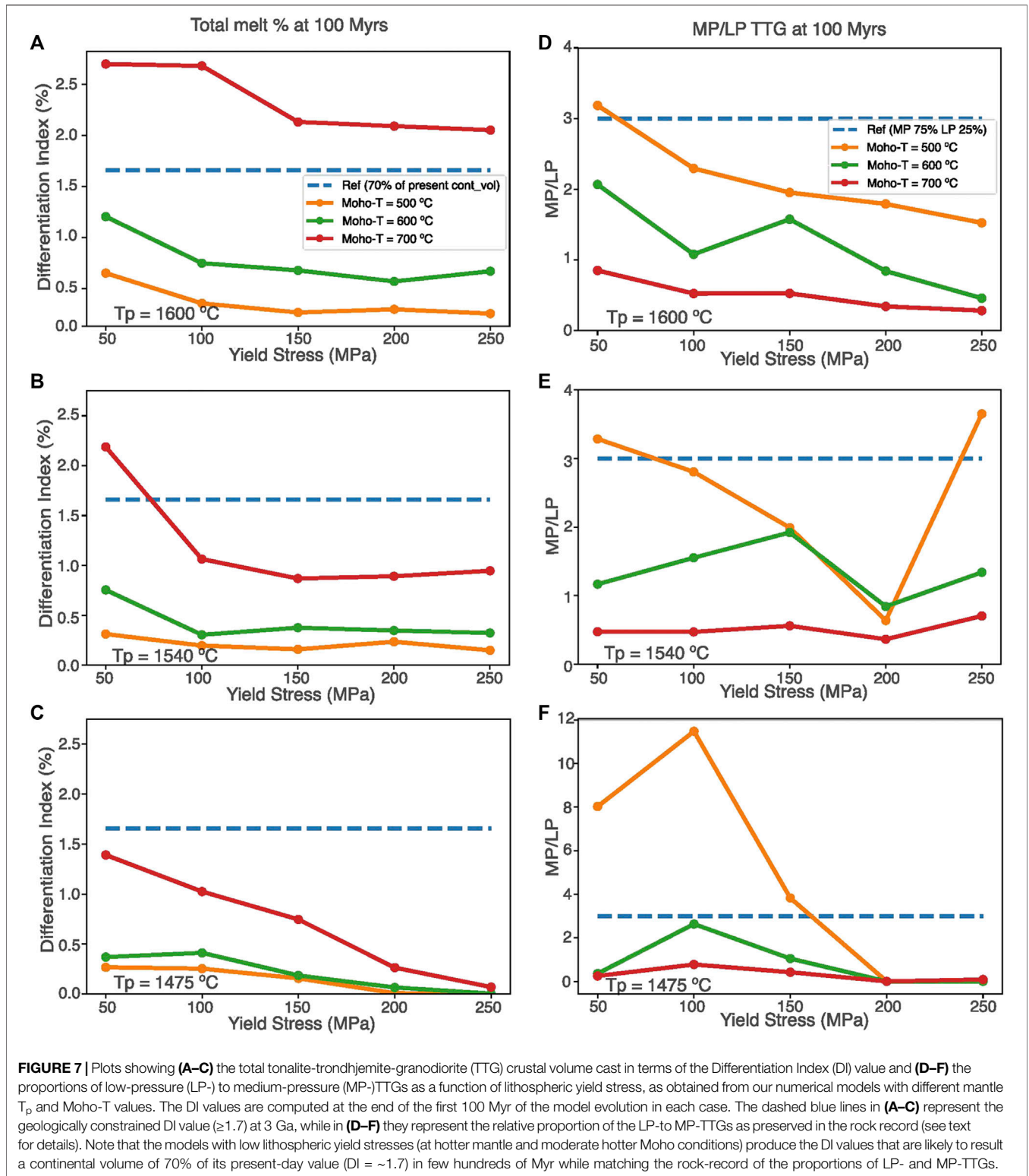
### Yield Stress of the Archean Lithosphere

Our modeling shows that Archean lithosphere has somewhat lower yield strength compared to the present-day lithosphere ( $>100\text{ MPa}$ ). The presence of such weaker lithosphere (together with hotter mantle) is critical for producing the large volumes of the Archean continental crust. This is because lowering the

lithospheric yield stress facilitate the dripping-off of basaltic crustal segments, where the most favourable melting conditions ( $\sim 0.7\text{--}1.8\text{ GPa}$ ;  $> 800^\circ\text{C}$ ) ascertained for the production of TTGs (e.g., Palin et al., 2016; Johnson et al., 2017; cf.; Moyen and Laurent, 2018), are easily attained. Furthermore, weaker lithosphere (with moderately high Moho-T) can aptly replicate the relative dominance of MP-TTGs over LP-TTGs similar to what is preserved in the rock-record. Higher values of yield stress ( $>100\text{ MPa}$ ) would impede the formation of drips and therefore, would result in a lower abundance of MP-TTGs, particularly if the crust is not significantly thick and/or thermally pre-conditioned for melting. Consequently, we suggest that the yield strength of Archean lithosphere likely varied between  $\sim 50$  and  $100\text{ MPa}$ , provided the mantle was significantly hotter than today.

The yield stress of material is temperature dependent in most engineering applications (Liu et al., 2002; Senkova et al.,





2006; Heidarzadeh et al., 2014; Wu et al., 2014; Altenberger et al., 2015), as well as geological laboratory experiments related to different rock compositions (Evans and Goetze., 1979; Long et al., 2011; Sygala et al., 2013; Idrissi et al., 2016; Hansen et al., 2019). Therefore, owing to the hotter thermal structure and different crustal composition of Archean lithosphere relative to the present-day crust (Chardon et al., 2009; Dhuime et al., 2015; Tang et al., 2016; Brown et al., 2020), it is expected to have a lower yield strength. In fact, studies of how a lithosphere deforms have shown that it involves three main mechanisms: diffusion creep, dislocation creep and Peierls mechanism (Regenauer-Lieb et al., 2006), and ultimately results in a shear heating controlled rupture of the ductile harder lithospheric layer (Regenauer-Lieb et al., 2001; Thielmann and Kaus, 2012; Stern and Gerya, 2018). The yield stress that we apply is an average of a large number of processes, which are primarily thermally controlled and secondary pressure controlled, and determine the rupture of a lithosphere whose ultimate strength is thermally controlled (Braeck and Podladchikov, 2007). Consequently, the effect on the thermally driven tectonic style during the Archean, when the uppermost mantle boundary layer was hotter, is expected.

The results agree with laboratory experiments of rock deformation showing a lower yield stress with increasing temperature (Evans and Goetze., 1979; Long et al., 2011; Sygala et al., 2013; Idrissi et al., 2016; Hansen et al., 2019). Postulations of weaker lithosphere due to hotter mantle temperatures, higher radioactive heat generation and melt impregnation have been suggested by previous studies as well (e.g., van Hunen and van den Berg, 2008; Sizova et al., 2010; Magni et al., 2014; Rozel et al., 2017). Our results converge with these studies in finding a need for a weaker lithospheric strength. Overall, the lithospheric weakening could have occurred due to both viscous strength variations as well as yield strength variations with higher temperature conditions in the Archean Earth.

## Tectonic Settings for the Early TTG Formation

Our modeling also bears implications for tectonic settings where the Archean felsic crust formation may have occurred. Previous studies have invoked both plate tectonic settings (mainly subduction) analogous to the present-day scenario (e.g., Foley et al., 2003; Harrison, 2009; Korenaga, 2018; Turner et al., 2020) or at various tectonic sites hosted within a stagnant-lid type tectonic regime (e.g., Smithies et al., 2009; Sizova et al., 2015; Johnson et al., 2017; Nebel et al., 2018; Smithies et al., 2019) for the formation of TTG-dominated crust during the Archean. Although the debate continues, recent studies are increasingly favoring the stagnant (squishy)-lid to transitional mobile-lid tectonic settings (not like *modern* plate tectonics) for the Archean crust formation (Johnson et al., 2014; Sizova et al., 2015; Chowdhury et al., 2017; Condie, 2017; Hawkesworth et al., 2017; Rozel et al., 2017; Johnson et al., 2017; Cawood et al., 2018; Moyen and Laurent, 2018; Capitanio et al., 2019; Smithies et al., 2019; Chowdhury et al., 2020). Tectonic processes like crustal thickening, dripping and local

crustal overturns are suggested as settings for TTG production, particularly during the pre-3 Ga time-period (e.g., Smithies, 2000; Johnson et al., 2014; Sizova et al., 2015; Johnson et al., 2017). Our study highlights the relative dominance of these different non-plate tectonic mechanisms in producing TTGs. The reference model shows that production of TTG dominantly occurs during the dripping phase instead of during the crustal thickening phase. This partly contradicts the results of Sizova et al. (2015), which showed that crustal thickening promotes TTG production. However, they implemented an unusually high, initial Moho-T of  $\sim 1,200^{\circ}\text{C}$ , which is markedly higher than  $600^{\circ}\text{C}$  value used in our model. Such lower Moho-T values together with the rapid transition of the thickened crustal domains into drips (within  $<10$  Myr) at low yield stresses, impeded large-scale melting of the mafic crust during crustal thickening in the reference model. This becomes evident when we increase the Moho-T and yield stress compared to the reference model and observed a greater proportion of melting within the thickened crustal domains.

Nonetheless, in all our models, the dripping process dominates TTG formation. We infer that this is because dripping continuously brings newer basaltic material to the melting region, maintaining a steady melting of the source rock (Figures 4 and 6). Secondly, dripping leads to crustal thinning and the resultant, mantle upwelling around the locale of the drip. This heats up the surrounding crust, which facilitates its subsequent melting. In contrast, only a thin layer of the lower most crust reaches melting conditions within a thickened crustal segment (Figures 6E,F). Given that crustal thickening occurs at a local scale and is not laterally pervasive, the resultant melting and TTG production is also limited. We, however, do not suggest that crustal thickening did not contribute toward Archean crustal growth. Instead, we imply that this may have contributed significantly only when an unusually hot (Moho-T  $> 1,000\text{--}1,200^{\circ}\text{C}$ ) and thick ( $>35\text{--}40$  km) mafic crust was available for melting conditions that may have existed in the Archean but perhaps not everywhere (cf. Cawood and Hawkesworth, 2019).

## CONCLUSIONS

The preserved record of early Archean felsic crust is more consistent with the presence of weaker lithosphere during active tectonism at those times. Tectonic activity involving such weaker lithosphere atop hotter mantle would have led to the production of voluminous TTG melt prior to  $\sim 3$  Ga, consistent with the inference of numerous crustal growth models. Our study further shows that TTG production may have dominantly occurred within mafic crustal drips, whereas crustal thickening made an only subordinate contribution unless the crust was significantly thicker. The low yield stress facilitated the drips to grow in length up to few hundreds of km and keeping them stable over tens of Myr. Furthermore, weaker lithosphere together with the dominance of dripping can also account for the large abundance of MP-TTGs relative to the LP-variant within the early Archean rock record.

## DATA AVAILABILITY STATEMENT

The raw data supporting the conclusions of this manuscript will be made available by the authors, without undue reservation, to any qualified researcher.

## AUTHOR CONTRIBUTIONS

PG—Overall research project is carried out from identifying the research problem, model development, and evaluation of results to drafting the manuscripts. GM—Provided support for the numerical model development, applying Geophysical significance, and Initial manuscript corrections. PC—Provided support in interpreting the model results, comparing them with the rock-record and manuscript development. PAC—The whole research project was guided by PAC from identifying the research problem to final manuscript development.

## REFERENCES

- Allègre, C. J., and Rousseau, D. (1984). The growth of the continent through geological time studied by Nd isotope analysis of shales. *Earth Planet. Sci. Lett.* 67 (1), 19–34.
- Altenberger, I., Kuhn, H.-A., Müller, H. R., Mhaede, M., Gholami-Kermanshah, M., and Wagner, L. (2015). Material properties of high-strength beryllium-free copper alloys. *Int. J. Mater. Prod. Technol.* 50 (2), 124–146. doi:10.1504/IJMPT.2015.067820
- Armstrong, R. L. (1981). Radiogenic isotopes: the case for crustal recycling on a near-steady-state no-continental-growth earth. *Phil. Trans. A Math. Phys. Sci.* 301 (1461), 443–472. doi:10.1098/rsta.1981.0122
- Artemieva, I. M. (2006). Global  $1^\circ \times 1^\circ$  thermal model TC1 for the continental lithosphere: implications for lithosphere secular evolution. *Tectonophysics* 416 (1–4), 245–277. doi:10.1016/j.tecto.2005.11.022
- Aulbach, S., and Arndt, N. T. (2019). Eclogites as palaeodynamic archives: evidence for warm (not hot) and depleted (but heterogeneous) Archaean ambient mantle. *Earth Planet. Sci. Lett.* 505, 162–172. doi:10.1016/j.epsl.2018.10.025
- Bédard, J. H. (2003). Evidence for regional-scale, pluton-driven, high-grade metamorphism in the archaean minto block, northern Superior province, Canada. *J. Geol.* 111, 183–205. doi:10.1086/345842
- Belousova, E. A., Kostitsyn, Y. A., Griffin, W. L., Begg, G. C., O'Reilly, S. Y., and Pearson, N. J. (2010). The growth of the continental crust: constraints from zircon Hf-isotope data. *Lithos* 119 (3–4), 457–466. doi:10.1016/j.lithos.2010.07.024
- Braeck, S., and Podladchikov, Y. Y. (2007). Spontaneous thermal runaway as an ultimate failure mechanism of materials. *Phys. Rev. Lett.* 98 (9), 095504. doi:10.1103/physrevlett.98.095504
- Brown, M., Johnson, T., and Gardiner, N. J. (2020). Plate tectonics and the archaean earth. *Annu. Rev. Earth Planet. Sci.* 48, 1–12. doi:10.1146/annurev-earth-081619-052705
- Campbell, I. H. (2003). Constraints on continental growth models from Nb/U ratios in the 3.5 Ga Barberton and other Archaean basalt-komatite suites. *Am. J. Sci.* 303 (4), 319–351. doi:10.2475/ajs.303.4.319
- Capitanio, F. A., Nebel, O., Cawood, P. A., Weinberg, R. F., and Chowdhury, P. (2019). Reconciling thermal regimes and tectonics of the early Earth. *Geology* 47, 923–927. doi:10.1130/g46239.1
- Cawood, P. A., and Hawkesworth, C. J. (2019). Continental crustal volume, thickness and area, and their geodynamic implications. *Gondwana Res.* 66, 116–125. doi:10.1016/j.gr.2018.11.001
- Cawood, P. A., Hawkesworth, C. J., and Dhuime, B. (2013). The continental record and the generation of continental crust. *Geol. Soc. Am. Bull.* 125 (1–2), 14–32. doi:10.1130/b30722.1
- Cawood, P. A., Hawkesworth, C. J., Pisarevsky, S. A., Dhuime, B., Capitanio, F. A., and Nebel, O. (2018). Geological archive of the onset of plate tectonics. *Philos. Trans. A Math. Phys. Eng. Sci.* 376 (2132), 20170405. doi:10.1098/rsta.2017.0405

## FUNDING

MIPRS and MGS PhD scholarship provided by Monash University, and Australian Research Council grant FL160100168.

## ACKNOWLEDGMENTS

We acknowledge the computational resources provided by the Monash eResearch Center and eSolutions-Research Support Services (for the MonARCH HPC Cluster) and National Computational Infrastructure (NCI), Australia. We thank Jeroen van Hunen (Durham University) and two reviewers for their constructive comments that have immensely improved the manuscript. We also thank Christopher M. Gonzalez, Shayne McGregor, Fabio Capitanio, and John Mansour (Monash University) for insightful discussions.

- Chardon, D., Gapais, D., and Cagnard, F. (2009). Flow of ultra-hot orogens: a view from the Precambrian, clues for the Phanerozoic. *Tectonophysics* 477, 105–118. doi:10.1016/j.tecto.2009.03.008
- Chowdhury, P., Chakraborty, S., Gerya, T. V., Cawood, P. A., and Capitanio, F. A. (2020). Peel-back controlled lithospheric convergence explains the secular transitions in Archean metamorphism and magmatism. *Earth Planet. Sci. Lett.* 538, 116224. doi:10.1016/j.epsl.2020.116224
- Chowdhury, P., Gerya, T., and Chakraborty, S. (2017). Emergence of silicic continents as the lower crust peels off on a hot plate-tectonic Earth. *Nat. Geosci.* 10, 698–703. doi:10.1038/ngeo3010
- Condie, K. C. (2017). A planet in transition: the onset of plate tectonics on Earth between 3 and 2 Ga? *Geosci. Front.* 9, 51–60. doi:10.1016/j.gsf.2016.09.001
- Condie, K. C., and Aster, R. C. (2010). Episodic zircon age spectra of orogenic granulites: the supercontinent connection and continental growth. *Precambrian Res.* 180 (3–4), 227–236. doi:10.1016/j.precamres.2010.03.008
- Dhuime, B., Hawkesworth, C. J., Cawood, P. A., and Storey, C. D. (2012). A change in the geodynamics of continental growth 3 billion years ago. *Science* 335, 1334–1336. doi:10.1126/science.1216066
- Dhuime, B., Wuestefeld, A., and Hawkesworth, C. J. (2015). Emergence of modern continental crust about 3 billion years ago. *Nat. Geosci.* 8 (7), 552–555. doi:10.1038/ngeo2466
- Evans, B., and Goetze, C. (1979). The temperature variation of hardness of olivine and its implication for polycrystalline yield stress. *J. Geophys. Res.* 84, 5505–5524. doi:10.1029/jb084ib10p05505
- Evans, M. W., and Harlow, F. H. (1957). *The particle-in-cell method for hydrodynamic calculations*. Los Angeles, CA: Los Alamos National Laboratory Report, 2139.
- Foley, S. F., Buhre, S., and Jacob, D. E. (2003). Evolution of the Archean crust by delamination and shallow subduction. *Nature* 421, 241–252. doi:10.1038/nature01319
- Fyfe, W. S. (1978). The evolution of the earth's crust: modern plate tectonics to ancient hot spot tectonics? *Chem. Geol.* 23 (1–4), 89–114. doi:10.1016/0009-2541(78)90068-2
- Ganne, J., and Feng, X. (2017). Primary magmas and mantle temperatures through time. *Geochem. Geophys. Geosyst.* 18, 872–888. doi:10.1002/2016gc006787
- Gerya, T. V. (2010). *Introduction to numerical geodynamic modelling*. New York, NY: Cambridge University Press.
- Gerya, T. V. (2019). Geodynamics of the early Earth: quest for the missing paradigm. *Geology* 47 (10), 1006–1007. doi:10.1130/focus-Oct2019
- Goodwin, A. M. (1996). *Principles of precambrian geology*. London, UK: Academic Press, 327.
- Gurnis, M. (1988). Large-scale mantle convection and the aggregation and dispersal of supercontinents. *Nature* 332 (6166), 695–699. doi:10.1038/332695a0
- Harrison, T. M. (2009). The Hadean crust: evidence from >4 Ga zircons. *Annu. Rev. Earth Planet. Sci.* 37, 479–505. doi:10.1146/annurev.earth.031208.100151

- Hansen, L. N., Kumamoto, K. M., Thom, C. A., Wallis, D., Durham, W. B., Goldsby, D. L., et al. (2019). Low-temperature plasticity in olivine: grain size, strain hardening, and the strength of the lithosphere. *J. Geophys. Res. Solid Earth* 124, 5427–5449. doi:10.1029/2018jb016736
- Hawkesworth, C. J., Cawood, P. A., Dhuime, B., and Kemp, T. I. S. (2017). Earth's continental lithosphere through time. *Annu. Rev. Earth Planet. Sci.* 45, 169–198. doi:10.1146/annurev-earth-063016-020525
- Heidarzadeh, A., Jabbari, M., and Esmaily, M. (2015). Prediction of grain size and mechanical properties in friction stir welded pure copper joints using a thermal model. *Int. J. Adv. Manuf. Technol* 77 (9–12), 1819–1829. doi:10.1007/s00170-014-6543-7
- Herzberg, C., Asimow, P. D., Arndt, N., Niu, Y., Leshner, C. M., Fitton, J. G., et al. (2007). Temperatures in ambient mantle and plumes: constraints from basalts, picrites and komatiites. *Geochem. Geophys. Geosyst.* 8, Q02006. doi:10.1029/2006gc001390
- Herzberg, C., Condie, K., and Korenaga, J. (2010). Thermal history of the Earth and its petrological expression. *Earth Planet. Sci. Lett.* 292, 79–88. doi:10.1016/j.epsl.2010.01.022
- Herzberg, C., and Rudnick, R. (2012). Formation of cratonic lithosphere: an integrated thermal and petrological model. *Lithos* 149, 4–15. doi:10.1016/j.lithos.2012.01.010
- Idrissi, H., Bollinger, C., Boioli, F., Schryvers, D., and Cordier, P. (2016). Low-temperature plasticity of olivine revisited with *in situ* TEM nanomechanical testing. *Sci. Adv.* 2, e1501671. doi:10.1126/sciadv.1501671
- Ito, K., and Kennedy, G. C. (1971). “An experimental study of the basalt-garnet granulite-eclogite transition.” in *The structure and physical properties of the Earth's crust*. Editor J. G. Heacock (American Geophysical Union), Vol. 14, 303–314.
- Jain, C., Rozel, A. B., Tackley, P. J., Sanan, P., and Gerya, T. V. (2019). Growing primordial continents self-consistently in global mantle convection models. *Gondwana Res.* 73, 96–122. doi:10.1016/j.gr.2019.03.015
- Johnson, T. E., Brown, M., Gardiner, N. J., Kirkland, C. L., and Smithies, R. H. (2017). Earth's first stable continents did not form by subduction. *Nature* 543, 239–242. doi:10.1038/nature21383
- Johnson, T. E., Brown, M., Kaus, B. J. P., and Van Tongeren, J. A. (2014). Delamination and recycling of Archaean crust caused by gravitational instabilities. *Nat. Geosci.* 7, 47–52. doi:10.1038/ngeo2019
- Kamber, B. S. (2015). The evolving nature of terrestrial crust from the Hadean, through the Archaean, into the Proterozoic. *Precambrian Res.* 258, 48–82. doi:10.1016/j.precamres.2014.12.007
- Kohlstedt, D. L., Evans, B., and Mackwell, S. J. (1995). Strength of the lithosphere: constraints imposed by laboratory experiments. *J. Geophys. Res.* 100, 17587–17602. doi:10.1029/95jb01460
- Korenaga, J. (2010a). On the likelihood of plate tectonics on super-Earths: does size matter? *Astrophys. J. Lett.* 725, L43–L46. doi:10.1088/2041-8205/725/1/L43
- Korenaga, J. (2010b). Scaling of plate-tectonic convection with pseudoplastic rheology. *J. Geophys. Res.* 115, B11405. doi:10.1029/2010jb007670
- Korenaga, J. (2013). Initiation and evolution of plate tectonics on Earth: theories and observations. *Annu. Rev. Earth Planet. Sci.* 41, 117–151. doi:10.1146/annurev-earth-050212-124208
- Korenaga, J. (2018). Crustal evolution and mantle dynamics through Earth history. *Philos. Trans. A Math. Phys. Eng. Sci.* 376 (2132), 20170408. doi:10.1098/rsta.2017.0408
- Lenardic, A. (2018). The diversity of volcanic-tectonic modes and thoughts about transitions between them. *Philos. Trans. A Math. Phys. Eng. Sci.* 376 (2132), 20170416. doi:10.1098/rsta.2017.0416
- Liu, Z. C., Lin, J. P., Li, S. J., and Chen, G. L. (2002). Effects of Nb and Al on the microstructures and mechanical properties of high Nb containing TiAl base alloys. *Intermetallics* 10, 653–659. doi:10.1016/s0966-9795(02)00037-7
- Long, H., Weidner, D. J., Li, L., Chen, J., and Wang, L. (2011). Deformation of olivine at subduction zone conditions determined from *in situ* measurements with synchrotron radiation. *Earth Planet. Sci. Lett.* 186, 23–35. doi:10.1016/j.pepi.2011.02.006
- Lowman, J. P., and Jarvis, G. T. (1999). Effects of mantle heat source distribution on supercontinent stability. *J. Geophys. Res.* 104 (6), 12733–12747. doi:10.1029/1999jb900108
- Magni, V., Bouilhol, P., and van Hunen, J. (2014). Deep water recycling through time. *Geochem. Geophys. Geosyst.* 15 (11), 4203–4216. doi:10.1002/2014GC005525
- Martin, H., and Moyen, J.-F. (2002). Secular changes in TTG composition as markers of the progressive cooling of the Earth. *Geology* 30 (4), 319–322. doi:10.1130/0091-7613(2002)030<0319:scittg>2.0.co;2
- McCoy-West, A. J., Chowdhury, P., Burton, K. W., Sossi, P., Nowell, G. M., Fitton, J. G., et al. (2019). Extensive crustal extraction in Earth's early history inferred from molybdenum isotopes. *Nat. Geosci.* 12, 946–951. doi:10.1038/s41561-019-0451-2
- Moresi, L., Quenette, S., Lemiale, V., Mériaux, C., Appelbe, B., and Mühlhaus, H. B. (2007). Computational approaches to studying non-linear dynamics of the crust and mantle. *Phys. Earth Planet. Inter.* 163 (1–4), 69–82. doi:10.1016/j.pepi.2007.06.009
- Moresi, L., and Solomatov, V. (1998). Mantle convection with a brittle lithosphere: thoughts on the global tectonic styles of the Earth and Venus. *Geophys. J. Int.* 133, 669–682. doi:10.1046/j.1365-246x.1998.00521.x
- Moyen, J.-F. (2011). The composite Archean grey gneisses: petrological significance, and evidence for a non-unique tectonic setting for Archean crustal growth. *Lithos* 123, 21–36. doi:10.1016/j.lithos.2010.09.015
- Moyen, J.-F., and Laurent, O. (2018). Archaean tectonic systems: a view from igneous rocks. *Lithos* 302 (303), 99–125. doi:10.1016/j.lithos.2017.11.038
- Moyen, J.-F., and Stevens, G. (2006). “Experimental constraints on TTG petrogenesis: implications for Archean geodynamics.” in *Archean geodynamics and environments*. Editors K. Benn, J. -C. Mareschal, and K. C. Condie (AGU), 149–178.
- Nebel, O., Capitanio, F. A., Moyen, J.-F., Weinberg, R. F., Clos, F., Nebel-Jacobsen, Y. J., et al. (2018). When crust comes of age: on the chemical evolution of Archaean, felsic continental crust by crustal drip tectonics. *Philos. Trans. A Math. Phys. Eng. Sci.* 376 (2132), 20180103. doi:10.1098/rsta.2018.0103
- O'Neill, C., and Lenardic, A. (2007). Geological consequences of super-sized Earths. *Geophys. Res. Lett.* 34, L19204. doi:10.1029/2007gl030598
- O'Neill, C., Marchi, S., Bottke, W., and Fu, R. (2020). The role of impacts on Archaean tectonics. *Geology* 48, 174–178. doi:10.1130/G46533.1
- Palin, R. M., White, R. W., and Green, E. C. R. (2016). Partial melting of metabasic rocks and the generation of tonalitic-trondhjemitic-granodioritic (TTG) crust in the Archaean: constraints from phase equilibrium modelling. *Precambrian Res.* 287, 73–90. doi:10.1016/j.precamres.2016.11.001
- Poudjom Djomani, Y. H., O'Reilly, S. Y., Griffin, W. L., and Morgan, P. (2001). The density structure of subcontinental lithosphere through time. *Earth Planet. Sci. Lett.* 184, 605–621. doi:10.1016/s0012-821x(00)00362-9
- Pujol, M., Marty, B., Burgess, R., Turner, G., and Philippot, P. (2013). Argon isotopic composition of Archaean atmosphere probes early Earth geodynamics. *Nature* 498, 87–90. doi:10.1038/nature12152
- Qian, Q., and Hermann, J. (2013). Partial melting of lower crust at 10–15 kbar: constraints on adakite and TTG formation. *Contrib. Mineral. Petrol.* 165, 1195–1224. doi:10.1007/s00410-013-0854-9
- Rapp, R. P., Shimizu, N., and Norman, M. D. (2003). Growth of early continental crust by partial melting of eclogite. *Nature* 425, 605–609. doi:10.1038/nature02031
- Regenauer-Lieb, K., Weinberg, R. F., and Rosenbaum, G. (2006). The effect of energy feedbacks on continental strength. *Nature* 442 (7098), 67–70. doi:10.1038/nature04868
- Regenauer-Lieb, K., Yuen, D. A., and Branlund, J. (2001). The initiation of subduction: critically by addition of water? *Science* 294, 578–580. doi:10.1126/science.1063891
- Rey, P. F., Coltice, N., and Flament, N. (2014). Spreading continents kick-started plate tectonics. *Nature* 513, 405–408. doi:10.1038/nature13728
- Roberts, N. M. W., and Spencer, C. J. (2015). The zircon archive of continent formation through time. *Geol. Soc. Lond. Spec. Publ.* 389 (1), 197–225. doi:10.1144/sp389.14
- Rosas, J. C., and Korenaga, J. (2018). Rapid crustal growth and efficient crustal recycling in the early Earth: implications for Hadean and Archean geodynamics. *Earth Planet. Sci. Lett.* 494, 42–49. doi:10.1016/j.epsl.2018.04.051
- Rozel, A. B., Golabek, G. J., Jain, C., Tackley, P. J., and Gerya, T. V. (2017). Continental crust formation on early Earth controlled by intrusive magmatism. *Nature* 545, 332–335. doi:10.1038/nature22042
- Rudnick, R. L., and Gao, S. (2003). “Composition of the continental crust,” in *Treatise on geochemistry*. Editors H. D. Holland and K. K. Turekian (Amsterdam, Netherlands: Elsevier), Vol. 3, 1–64. doi:10.1016/B0-08-043751-6/03016-4
- Schmeling, H. (2006). A model of episodic melt extraction for plumes. *J. Geophys. Res.* 111, B03202. doi:10.1029/2004jb003423
- Senkova, S. V., Senkov, O. N., and Miracle, D. B. (2006). Cryogenic and elevated temperature strengths of an Al–Zn–Mg–Cu alloy modified with Sc and Zr. *Metall. Mater. Trans. A* 37, 3569–3575. doi:10.1007/s11661-006-1051-5

- Sizova, E., Gerya, T., Brown, M., and Perchuk, L. L. (2010). Subduction styles in the Precambrian: insight from numerical experiments. *Lithos* 116, 209–229. doi:10.1016/j.lithos.2009.05.028
- Sizova, E., Gerya, T., Stüwe, K., and Brown, M. (2015). Generation of felsic crust in the Archean: a geodynamic modeling perspective. *Precambrian Res.* 271, 198–224. doi:10.1016/j.precamres.2015.10.005
- Smithies, R. H. (2000). The Archean tonalite–trondhjemite–granodiorite (TTG) series is not an analogue of Cenozoic adakite. *Earth Planet. Sci. Lett.* 182, 115–125. doi:10.1016/s0012-821x(00)00236-3
- Smithies, R. H., Champion, D. C., and Van Kranendonk, M. J. (2009). Formation of Paleoproterozoic continental crust through infracrustal melting of enriched basalt. *Earth Planet. Sci. Lett.* 281, 298–306. doi:10.1016/j.epsl.2009.03.003
- Smithies, R. H., Ivanic, T. J., Lowrey, J. R., Morris, P. A., Barnes, S. J., Wyche, S., et al. (2018). Two distinct origins for Archean greenstone belts. *Earth Planet. Sci. Lett.* 487, 106–116. doi:10.1016/j.epsl.2018.01.034
- Smithies, R. H., Lu, Y., Johnson, T. E., Kirkland, C. L., Cassidy, K. F., Champion, D. C., et al. (2019). No evidence for high-pressure melting of Earth's crust in the Archean. *Nat. Commun.* 10, 5559. doi:10.1038/s41467-019-13547-x
- Stern, R. J. (2018). The evolution of plate tectonics. *Philos. Trans. A Math. Phys. Eng. Sci.* 376 (2132), 20170406. doi:10.1098/rsta.2017.0406
- Stern, R. J., and Gerya, T. (2018). Subduction initiation in nature and models: a review. *Tectonophysics* 746, 173–198. doi:10.1016/j.tecto.2017.10.014
- Sygała, A., Bukowska, M., and Janoszek, T. (2013). High temperature versus geomechanical parameters of selected rocks—the present state of research. *J. Sustain. Min.* 12 (4), 45–51. doi:10.7424/jsm130407
- Tackley, P. J. (2000). Self-consistent generation of tectonic plates in time-dependent, three-dimensional mantle convection simulations, 1, Pseudoplastic yielding. *Geochem. Geophys. Geosyst.* 1 (8), 200GC000036. doi:10.1029/2000gc000036
- Tackley, P. J. (2000a). “The quest for self-consistent incorporation of plate tectonics in mantle convection,” in *History and dynamics of global plate Motions*. Editor M. A. Richards (AGU).
- Tang, M., Chen, K., and Rudnick, R. L. (2016). Archean upper crust transition from mafic to felsic marks the onset of plate tectonics. *Science* 351, 372–375. doi:10.1126/science.aad5513
- Thielmann, M., and Kaus, B. J. P. (2012). Shear heating induced lithospheric-scale localization: does it result in subduction? *Earth Planet. Sci. Lett.* 359 (360), 1–13. doi:10.1016/j.epsl.2012.10.002
- Trompert, R., and Hansen, U. (1998). Mantle convection simulations with rheologies that generate plate-like behaviour. *Nature* 395, 686–689. doi:10.1038/27185
- Turner, S., Wilde, S., Wörner, G., Schaefer, B., and Lai, Y.-J. (2020). An andesitic source for Jack Hills zircon supports onset of plate tectonics in the Hadean. *Nat. Commun.* 11, 1241. doi:10.1038/s41467-020-14857-1
- van Heck, H. J., and Tackley, P. J. (2008). Planforms of self-consistently generated plates in 3-d spherical geometry. *Geophys. Res. Lett.* 35, L19312. doi:10.1029/2008gl035190
- van Heck, H. J., and Tackley, P. J. (2011). Plate tectonics on super-earths: equally or more likely than on earth. *Earth Planet. Sci. Lett.* 310 (3–4), 252–261. doi:10.1016/j.epsl.2011.07.029
- van Hunen, J., and van den Berg, A. P. (2008). Plate tectonics on the early Earth: limitations imposed by strength and buoyancy of subducted lithosphere. *Lithos* 103 (1–2), 217–235. doi:10.1016/j.lithos.2007.09.016
- Wu, Z., Bei, H., Pharr, G. M., and George, E. P. (2014). Temperature dependence of the mechanical properties of equiatomic solid solution alloys with face-centered cubic crystal structures. *Acta Mater.* 81, 428e441. doi:10.1016/j.actamat.2014.08.026
- Zhang, C., Holtz, F., Koepke, J., Wolff, P. E., Ma, C., and Bédard, J. H. (2013). Constraints from experimental melting of amphibolite on the depth of formation of garnet-rich restites, and implications for models of Early Archean crustal growth. *Precambrian Res.* 231, 206–217. doi:10.1016/j.precamres.2013.03.004

**Conflict of Interest:** The authors declare that the research was conducted in the absence of any commercial or financial relationships that could be construed as a potential conflict of interest.

Copyright © 2020 Gunawardana, Morra, Chowdhury and Cawood. This is an open-access article distributed under the terms of the Creative Commons Attribution License (CC BY). The use, distribution or reproduction in other forums is permitted, provided the original author(s) and the copyright owner(s) are credited and that the original publication in this journal is cited, in accordance with accepted academic practice. No use, distribution or reproduction is permitted which does not comply with these terms.

## APPENDIX

### Appendix A1: Pressure-Temperature Conditions for Low-P, Medium-P and High-P TTG Formation

The pressure-temperature ( $P$ - $T$ ) conditions of LP- and MP-TTGs formation during the Archean (Figure 2) can be written as the following functions (Jain et al., 2019):

$$760 - 60(P - 1)^2 < T < 1,000 - 150\left(\frac{P - 1.2}{1.2}\right)^2 \quad (A1)$$

$$-0.5\left(\frac{T - 870}{220}\right) < P < 1.5 + 0.7\left(\frac{T - 700}{200}\right) \quad (A2)$$

where,  $T$  is in °C and  $P$  is in GPa. Low- $P$  TTGs generally forms at  $P < 0.8$ – $1$  GPa while the medium- $P$  TTGs forms at  $P > 0.7$ – $1$  GPa, depending upon the actual source rock composition (Moyen, 2011; Palin et al., 2016; Johnson et al., 2017). For simplicity, our employed

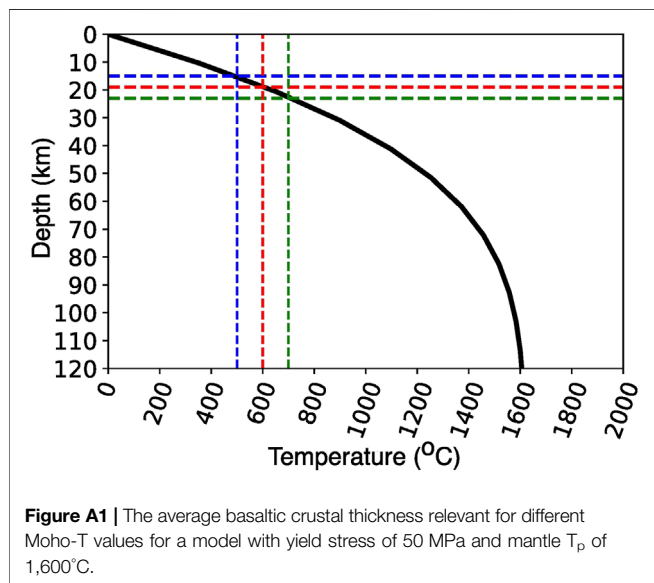


**Figure A1** | The average basaltic crustal thickness relevant for different Moho- $T$  values for a model with yield stress of 50 MPa and mantle  $T_p$  of 1,600°C.

**TABLE A1** | Melt extraction threshold values.

Material	M1	M2	M3	M4
Peridotite	0.00	0.05	0.4	0.4
Hydrated basalt	0.02	0.04	0.4	0.4

functions put this pressure bracket between low- $P$  and medium- $P$  TTGs at 1 GPa, following the traditional definition scheme put forward by Moyen (2011). The  $P$ - $T$  conditions for forming the High- $P$  TTG via partial melting of basalts is given by (Jain et al., 2019):

$$1,000 < T < 1,100 + 50\left(\frac{P - 3.5}{3.5}\right)^2 \quad (A3)$$

$$2.35 + 0.15\left(\frac{T - 1,000}{100}\right) < P < 2.5 \quad (A4)$$

### Appendix A2: Solidii and Liquidii for Different Lithologies Used in the Modeling

For mantle melting, we used the  $P$ - $T$  dependent peridotite melting model parametrized in Sizova et al. (2015).

$$T_{sol} = 1120.85 + 133P - 5.1P^2 \quad (A5)$$

$$T_{liq} = 1799.85 + 114P \quad (A6)$$

where  $P$  is in GPa and  $T$  is in °C. For the melting of hydrated basalt, we used the following parametrized solidus and liquidus functions (Sizova et al., 2015):

For,  $P < 1.6$  GPa

$$T_{sol} = 699.85 - \frac{70,400}{1,000P + 354} + \frac{77,800,000}{(1,000P + 354)^2} \quad (A7)$$

$$T_{liq} = 1149.85 + 105P \quad (A8)$$

for,  $1.6 \text{ GPa} < P < 10 \text{ GPa}$

$$T_{sol} = 661.85 + 3.5P + 6.2P^2 \quad (A9)$$

$$T_{liq} = 1149.85 + 105P \quad (A10)$$